Use of (Nd, Pr) sulphates obtained from electronic scrap as corrosion inhibitors for a C-Mn steel in 3.5 NaCl

R. Vazquez-Ramirez,[1] G. Salinas-Solano,[1] J. Porcayo-Calderon[1,2] and J.G. Gonzalez-Rodriguez[1]*

[1]Universidad Autonoma del Estado de Morelos, CIICAp, Av. Universidad 1001, 62209-Vuernavaca, Mor., Mexico
[2]Departamento de Ingeniería Química y Metalurgia, Universidad de Sonora, Hermosillo, Sonora 83000, Mexico
E-mail: ggonzalez@uaem.mx

Abstract

A rare earth-containing sulfate obtained from permanent magnets has been evaluated as a corrosion inhibitor for a C-Mn steel in 3.5% NaCl solution. The electrochemical techniques used include potentiodynamic polarization, linear polarization resistance and electrochemical impedance spectroscopy measurements. The inhibitor obtained is not a pure compound but a mixture of neodymium and praseodymium sulphates, in a proportion of *ca*. 65:35. The open circuit potential value shifts towards more cathodic values during the first 2 hours, but it moves towards more anodic values after this time until it reaches a relatively constant value, indicating the formation of a protective layer. The results show that this compound is a good corrosion inhibitor, with an efficiency that increases with time and its concentration up to 500 ppm, but decreases with a further increase in its concentration. The inhibitor does not induce the formation of a passive layer but the polarization resistance values increase almost 10-fold upon addition of the inhibitor. Although the compound affects both the anodic and cathodic electrochemical reactions, it has a stronger effect on the cathodic reaction. It forms a film of protective corrosion products by chemical adsorption on the steel surface following the Langmuir adsorption isotherm. The corrosion mechanism is controlled by charge transfer and remains unaltered with addition of the inhibitor.

Keywords: *rare earths, electronic scrap, corrosion inhibitor.*

Received: October 7, 2020. Published: April 19, 2021 doi: 10.17675/2305-6894-2020-10-2-8

1. Introduction

Metal corrosion causes both big economic losses in the industry and numerous accidents [1]. One of the most widely used methods to fight corrosion is to use corrosion inhibitors, although some of them are highly toxic, expensive and not friendly to the environment. For this reason, in the last decades a lot of effort has been done to develop new corrosion inhibitors that are environmentally friendly, such as compounds extracted from roots, leaves, and fruits [2–6]. In this sense, some lanthanides have been used as corrosion inhibitors for

various metals and alloys due to their low toxicity both to humans and to the environment [7–9].

It has been reported that the use of some Ce or La chlorides or nitrates as corrosion inhibitors in solutions containing chlorides, due to the formation of protective layers consisting of hydrated oxides, decreased the oxygen reduction reaction, the free corrosion potential, E_{corr}, and the corrosion current density, I_{corr} [10–15]. More recently, Somers [6] used rare earth 3-(4-methylbenzoyl)propionate salts (mbp), where the rare earths includes La, Ce, Nd and Y, and estimated them as corrosion inhibitors for mild steel in 0.01 M NaCl. All the compounds decreased the corrosion current density, I_{corr}, and acted as predominantly anodic inhibitors. Similarly, Peng [17] used La and Y 3-(4-methylbenzoyl)propionates with for AS1020 mild steel in 0.01 M NaCl solution finding that the inhibition performance is due to the establishment of a protective film. Similarly, Mohammedi [18] evaluated the use of $Y(NO_3)_3 \cdot 6H_2O$ and $CeCl_3 \cdot 7H_2O$ in conjunction with metasilicates ($Na_2SiO_3 \cdot 5H_2O$) as corrosion inhibitors for carbon A37 steel in aerated 3%NaCl solutions, finding that both anodic and cathodic reactions were inhibited leading to a decrease in the corrosion rate. Similar results were obtained for Mg and Al alloys in NaCl solutions [14, 19]. Besides the use of rare earths as corrosion inhibitors, they play an essential role in permanent magnets, lamp phosphors, catalysts, rechargeable batteries *etc*. China is the country that produces more than 90% of their global production whereas the rest of the world is confronted with a rare earths supply risk [20–22]. Thus, these countries will have to rely on recycling of rare earths from pre-consumer scrap and industrial residues that contain these elements. This paper deals with the use of recycled rare earth elements from permanent magnets, in particular (Nd, Pr) sulphates, as corrosion inhibitors for a C-Mn Steel in chloride solutions.

2. Experimental procedure

2.1 Preparation of a rare earth containing inhibitor

The used permanent magnets contained 60–70 wt.% Fe-Nd-1B with a total amount of Pr and Nd between 20–40% as described elsewhere [23]. The preparation of rare earths-containing sulphates started with a demagnetization process as described in [23] by heating the magnets at 300°C for 2 hours followed by crushing until a particle size of 0.5 mm in average was obtained. The following procedure is similar to that described in [23] but instead of using 36% v/v HCl, diluted sulfuric acid was used. The rare earths sulphate thus obtained was dried at 60°C for 2 hours. They were characterized by the X-ray diffraction technique on a Phillips X-ray diffractometer with Cu-Kα_1 radiation. The wavelength used to collect the intensity data was 1.5406 angstroms. The acceleration voltage and the current density used were 40 kV and 25 mA, respectively. The measurements were made in a 2θ range from 20° to 70° with a step of 0.0203°.

2.2 Electrochemical techniques

The working electrode was a C-Mn steel containing, in wt.%: Fe – 0.14 C – 0.90 Mn – 0.30 S – 0.30 P. Specimens were encapsulated in a commercial polymeric resin leaving an exposed area of 1.0 cm^2. Potentiodynamic polarization curves, linear polarization resistance (LPR) and electrochemical impedance spectroscopy (EIS) techniques were employed to evaluate the inhibitors obtained in 3.5 wt.% NaCl solution. In addition to these techniques, the variation in the open circuit potential value (OCP) was monitored throughout the tests. A naturally aerated three electrode glass cell was used, for which an Ag/AgCl and a graphite rod were used as the reference and auxiliary electrodes, respectively. Polarization curves were started once the free corrosion potential value, E_{corr}, was stable, approximately after 30 minutes, by polarizing a specimen from the cathodic to the anodic direction at a scan rate of 1 mV/s, starting at a potential value of 500 mV more cathodic than E_{corr}, and finishing the scanning at 800 mV more anodic than E_{corr}. The Tafel extrapolation method was used to calculate the corrosion current density value, I_{corr}. Inhibitor efficiency, *I.E.*, was calculated by the following equation:

$$I.E.(\%) = (I_{corr} - I_{corrinh})/I_{corr} \cdot 100 \quad (1)$$

where I_{corr} and $I_{corrinh}$ are the corrosion current densities without and with the inhibitor, respectively. For the LPR measurements, specimens were polarized ±15 mV around the E_{corr} value at a scanning rate of 1 mV/s every 60 minutes for 24 hours. Finally, EIS measurements were performed by applying a sinusoidal signal with an amplitude peak-to-peak of ±15 mV at the E_{corr} value in a frequency range of 0.01–100,000 Hz. EIS tests lasted for 24 hours. Selected corroded specimens were analysed in a scanning electronic microscope (SEM) whereas micro chemical analysis was performed with an X-ray energy dispersion (EDS) unit attached to the SEM.

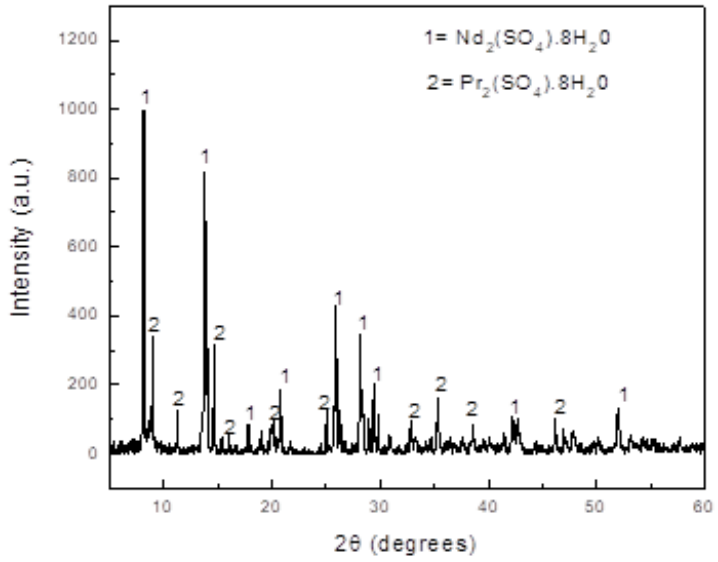

Figure 1. X-ray pattern of the rare earth-containing sulfate obtained from permanent magnets.

3. Results and Discussion

3.1 Inhibitor characterization

The corresponding X-ray pattern of the salts obtained is shown in Figure 1, where it can be seen that we are not dealing with a pure compound but with a mixture of neodymium and praseodymium sulphates, in a ratio of *ca*. 65:35. Similar results were reported by Olafsen [24] who obtained a complex oxide, $Pr_{2-x}Nd_xO_3$, from a La–Nd–O system and by Porcayo-Calderon [23] who reported a synthesis of a mixture of both neodymium and praseodymium chlorides.

3.2 Electrochemical results

The variation in the open circuit potential value, OCP, as a function of the inhibitor concentration for the C-Mn steel in 3.5 NaCl solution is shown in Figure 2. In the uninhibited solution (blank), the OCP shifted towards more cathodic values for the first 2 hours, however, it moved towards more anodic values after that time, until it reached a relatively constant value. The shift in the OCP value in the cathodic direction is due to the dissolution of the steel or any pre-existing film on its surface, whereas the shift towards more anodic values is due to the formation of a layer of corrosion products on its surface [25].

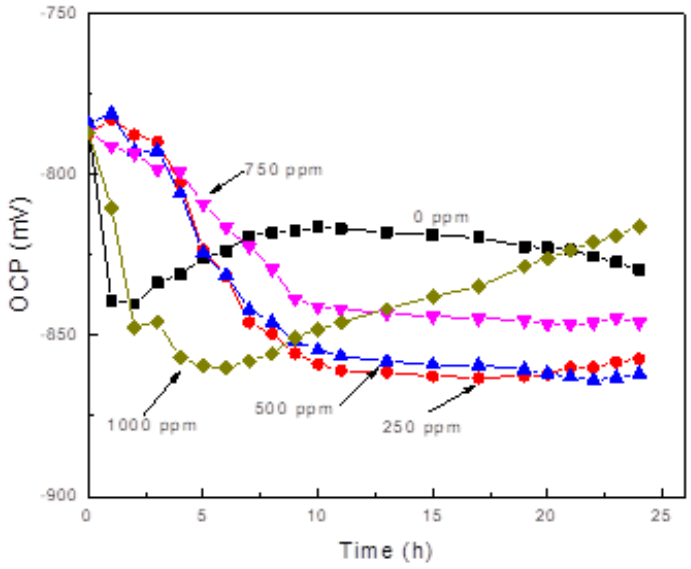

Figure 2. Effect of the inhibitor concentration on the OCP value for a C-Mn steel immersed in 3.5% NaCl solution.

When the inhibitor is added to the solution at a concentration lower than or equal to 750 ppm, the OCP shifts towards more cathodic ones, but it never changes this trend to the anodic direction, indicating that the steel does not develop a layer of protective corrosion products. When 1000 ppm of inhibitor are added, the OCP value has a similar behaviour to

that observed in the uninhibited solution, *i.e.* it moves to more cathodic values in the first 5 or 6 hours of testing, indicating steel dissolution, but after this time the OCP shifts to the anodic direction, indicating the formation of a protective layer of corrosion products [26].

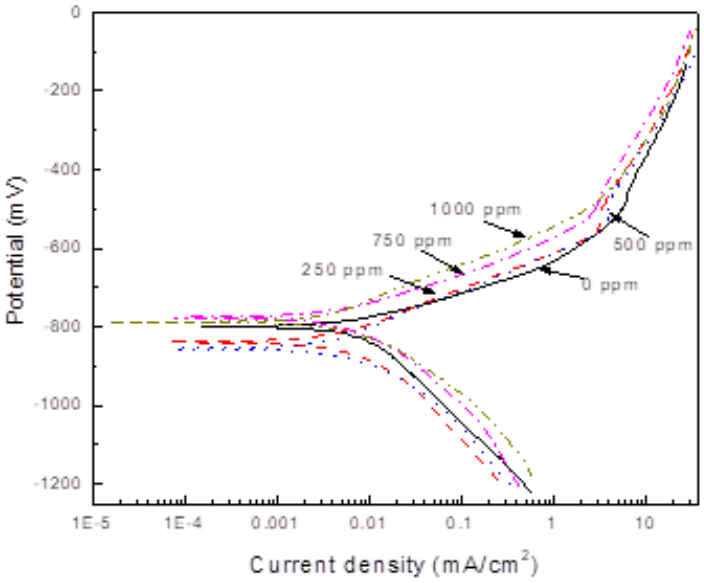

Figure 3. Effect of the inhibitor concentration on the polarization curves for a C-Mn steel immersed in 3.5% NaCl solution.

The polarization curves for C-Mn steel in 3.5 NaCl without and with the addition of various inhibitor concentrations are given in Figure 3 whereas the electrochemical parameters obtained from these curves are given in Table 1. It is clear from Figure 1 that the polarization curves do not display a passive zone but an active behaviour only. The E_{corr} value is shifted towards more cathodic values upon addition of either 250 or 500 ppm of the inhibitor as compared with the value for the uninhibited solution, whereas at inhibitor concentrations of 750 or 1000 ppm, E_{corr} is shifted towards nobler values. On the other hand, the corrosion current density value decreases gradually as the inhibitor concentration is increased, reaching its lowest value with the addition of 500 ppm, and it decreased once again with a further increase in the inhibitor concentration.

The inhibitor efficiency value increased with an increase in the inhibitor concentration, reaching its highest value with an inhibitor concentration of 500 ppm but decreasing with a further increase in the inhibitor concentration. Both anodic and cathodic Tafel slopes decreased with addition of the inhibitor, however, the cathodic slopes were affected more significantly than the anodic ones, indicating that this inhibitor acts as a mixed type inhibitor with a more predominant cathodic effect, thus affecting both anodic (steel dissolution) and cathodic hydrogen evolution and oxygen reduction reactions. This decrease in the corrosion rate is due to the adsorption of the inhibitor onto the steel surface since the surface area covered by the inhibitor, θ, which is obtained by dividing the inhibitor efficiency by 100,

increases as the inhibitor concentration increases to reach its highest value at an inhibitor concentration of 500 ppm, then decreases with a further increase in the inhibitor concentration.

Table 1. Electrochemical parameters obtained from polarization curves for the C-Mn steel immersed in 3.5% NaCl solution containing a rare earth-based inhibitor.

C_{inh} (ppm)	E_{corr} (mV)	I_{corr} (mA/cm^2)	β_a (mV/dec)	β_c (mV/dec)	*I.E.* (%)	θ
0	–800	$8\cdot10^{-3}$	70	235	–	–
250	–840	$6\cdot10^{-3}$	62	225	25	0.25
500	–855	$3\cdot10^{-3}$	53	190	63	0.63
750	–755	$4\cdot10^{-3}$	60	200	50	0.50
1000	–790	$5\cdot10^{-3}$	72	210	37	0.37

The way that rare earths decrease the I_{corr} values is by adsorbing on the steel surface, and, in order to know the way they are adsorbed various adsorption isotherms were used. As it can be seen from Figure 4, the Langmuir adsorption isotherm showed the best R^2 value, 0.99. The Langmuir adsorption isotherm is given by:

$$C_{inh}/\theta = 1/K_{ads} + C_{inh} \quad (2)$$

where C_{inh} is the inhibitor concentration, θ the surface metal area covered by the inhibitor which is obtained by dividing the inhibitor efficiency by 100, and K_{ads} is the adsorption constant of the process and can be obtained from the intercept of the data plotted in Figure 4 and is related to the adsorption free energy, ΔG_{ads} as follows:

$$\Delta G_{ads} = -RT \ln(10^6 K_{ads}) \quad (3)$$

The ΔG_{ads} value obtained was –48.56 kJ/mol, which indicates a strong chemical type of adsorption of the rare earth-based inhibitor on the steel metal [30].

Polarization curves represent a kind of instant picture which only give a description of the electrochemical reactions taking place on the metal surface at that specific moment. In order to evaluate the effect of the inhibitor on the corrosion rate decrease with time, Figure 5 depicts the change in the polarization resistance value, R_p, as a function of time at various inhibitor concentrations. For the uninhibited solution, the R_p value is the lowest and remains more or less constant with the passage of time. However, when the inhibitor is added, the R_p value starts to increase with time due to the formation of a corrosion products layer, and after some time it reaches a steady state value, indicating a more or less stable film of corrosion products. The R_p increases with the inhibitor concentration, reaching its highest value at an inhibitor concentration of 500 ppm, a value 8 times higher than that obtained for the uninhibited solution, and it decreases with a further increase in the inhibitor concentration.

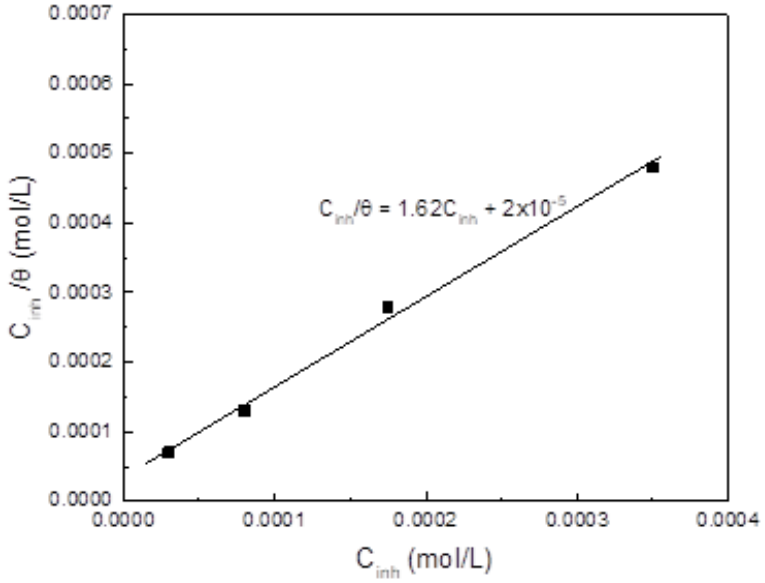

Figure 4. Langmuir adsorption isotherm on a C-Mn steel immersed in 3.5% NaCl solution containing a rare earth-based inhibitor.

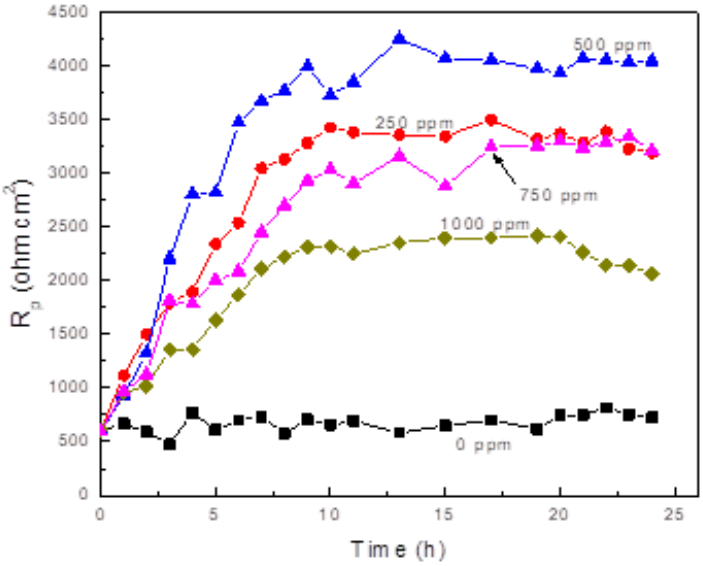

Figure 5. Effect of the inhibitor concentration on the R_p value for a C-Mn steel immersed in 3.5% NaCl solution.

Based on LPR data, the variation of the inhibitor efficiency value, *I.E.*, as a function of time can be calculated using the following expression:

$$I.E. = (R_{p/inh} - R_p)/R_{p/inh} \cdot 100 \quad (5)$$

where $R_{p/inh}$ and R_p represent the polarization resistance with and without the inhibitor, respectively. The results are given in Figure 6, and it is clear that the inhibitor efficiency increases with time regardless of the inhibitor concentration, due to an increase in the metal

surface area covered by the inhibitor. The highest inhibitor efficiency value, as expected, was obtained at an inhibitor concentration of 500 ppm, decreasing with a further increase in its concentration.

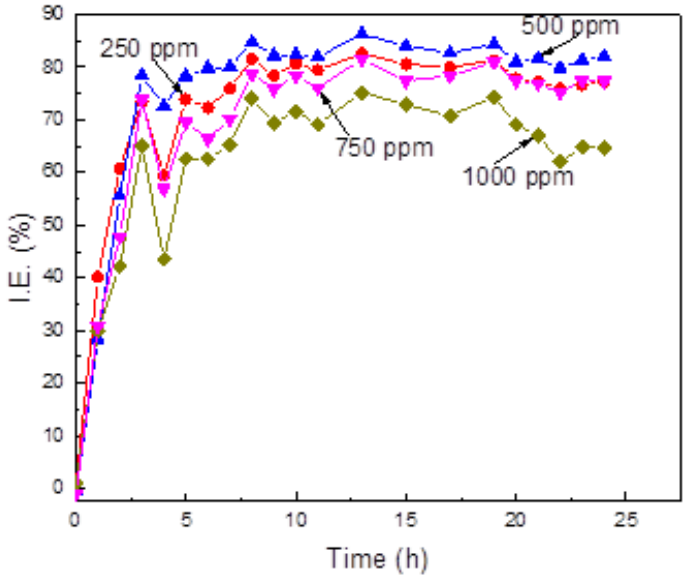

Figure 6. Effect of inhibitor concentration on the inhibitor efficiency as a function of time for a C-Mn steel immersed in 3.5% NaCl solution.

Similar results were obtained by EIS measurements. Figure 7 shows both Nyquist and Bode plots for the C-Mn steel corroding in 3.5 NaCl solution containing various concentrations of the rare earths based inhibitor. The Nyquist plots, Figure 7a, show a single depressed capacitive semicircle with its center at the real axis at all frequency values, indicating that the corrosion mechanism remains unchanged with the inhibitor concentration. The semicircle diameter increases as the inhibitor concentration increases, reaching its highest value at an inhibitor concentration of 500 ppm, and decreases with a further increase in the inhibitor concentration, in agreement with polarization curves and LPR results given above. On the other hand, the Bode plots in the modulus–frequency format, Figure 7b, show that the impedance modulus increases as the inhibitor concentration increases, reaching its highest value at 500 ppm of the inhibitor, and decreases when the inhibitor concentration is increased further. Two different slopes are observed in these plots, indicating the presence of two time constants. Similarly to this, the phase angle plots, Figure 7b, indicate only one peak for the uninhibited solution, and thus, only one time constant, which indicates that under these conditions, the formed layer of corrosion products is of non-protective nature; on the other hand, the solutions in the presence of the inhibitor show two peaks, and thus, two time constants, one related to the double electrochemical layer, and another one related to the corrosion products layer.

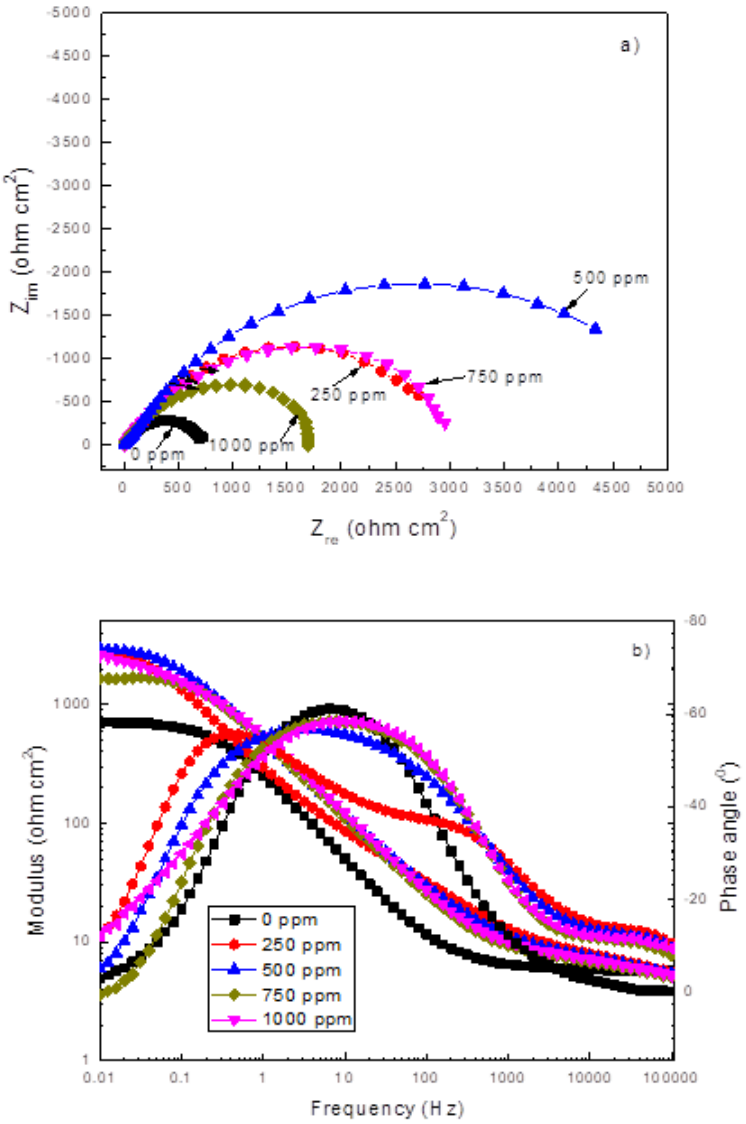

Figure 7. EIS data in the a) Nyquist and b) Bode format for a C-Mn steel immersed in 3.5% NaCl solution containing various concentrations of rare earth-based inhibitor.

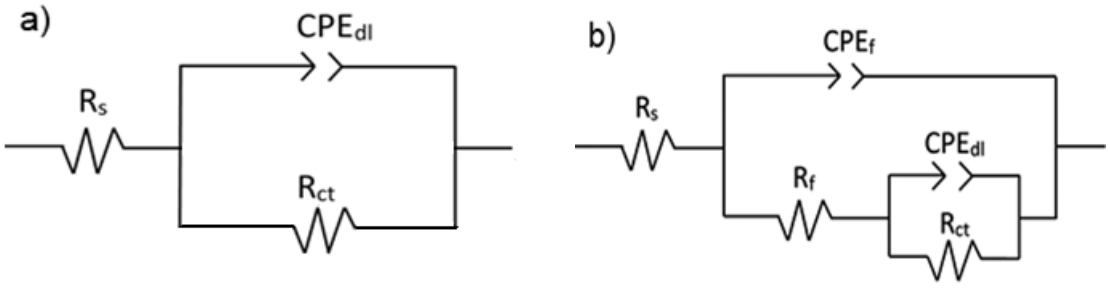

Figure 8. Electric circuits used to simulate EIS data for a C-Mn steel immersed in 3.5% NaCl solution a) in the absence and b) in the presence of the rare earth-based inhibitor.

Figure 8 displays the equivalent circuits used to simulate the experimental data obtained from the EIS plots for the C-Mn steel immersed in 3.5% NaCl solution with various concentrations of rare earth-based inhibitor. In these circuits, R_s represents the solution resistance, R_{ct} the charge transfer resistance that refers to the electrochemical process taking place at the metal/double electrochemical layer interface, C_{dl} the capacitance of the double electrochemical layer, R_f the corrosion products resistance that represents the electrochemical reactions taking place at the corrosion products/metal interface, and C_{ox} is the capacitance of the corrosion products. The capacitances were replaced by a constant phase element, CPE, considering the nonhomogeneous behavior of the interface as it is given by [26]:

$$Z_{CPE} = \frac{1}{Y(jw)^n} \tag{6}$$

where Y is the admittance, and n is related to the surface roughness and to the angle rotation of a pure capacitance, and it takes the values described in the paragraphs above into account.

The parameters obtained to fit the EIS data by the electric circuits shown in Figure 8 are given in Table 2. As can be seen from this table, the resistance of the corrosion products layer, R_f, is much larger than that of R_{ct}, indicating that the corrosion resistance is given by this layer. It is generally accepted that the first step during the adsorption of an inhibitor on a metal surface usually involves replacement of water molecules absorbed on the metal surface:

$$Inh_{sol} + xH_2O_{ads} \rightarrow Inh_{ads} + xH_2O_{sol} \tag{7}$$

The inhibitor may then combine with freshly generated Fe^{2+} ions on the steel surface, forming a metal-inhibitor complex:

$$Fe \rightarrow Fe^{2+} + 2e \tag{8}$$

$$Fe^{2+} + Inh_{ads} \rightarrow [Fe\text{-}Inh]_{ads}^{2+} \tag{9}$$

Table 2. Electrochemical parameters used to simulate the EIS data for a C-Mn steel immersed in 3.5% NaCl solution containing a rare earth-based inhibitor using the electrics circuit shown in Figure 8.

C_{inh} (ppm)	R_s (Ohm·cm^2)	R_{ct} (Ohm·cm^2)	CPE_{ct} (Ohm^{-1}·m^{-2}·s^n)	n_{ct}	R_f (Ohm·cm^2)	CPE_f (Ohm^{-1}·m^{-2}·s^n)	n_f
0	5	755	$8.0\cdot10^{-4}$	0.6	–	–	–
250	4	4.6	$1.1\cdot10^{-4}$	0.7	3108	$9.6\cdot10^{-4}$	0.8
500	2	4.4	$7.1\cdot10^{-5}$	0.9	5340	$4.1\cdot10^{-5}$	0.9
750	4	2.3	$2.7\cdot10^{-4}$	0.7	2736	$1.9\cdot10^{-4}$	0.7
1000	3	4.8	$6.4\cdot10^{-4}$	06	1786	$6.5\cdot10^{-4}$	0.6

The resulting complex can either inhibit further metal dissolution. Additionally, the R_f value increases with the inhibitor concentration to reach its highest value at an inhibitor concentration of 500 ppm, decreasing with a further increase in the inhibitor concentration. The CPE_f value decreases as the inhibitor concentration increases to reach its lowest value when 500 ppm of the inhibitor is added, and it increases with a further increase in the inhibitor concentration. Finally an *n* value close to 1.0 indicates a low steel surface roughness due to a low metal dissolution, thus, a low corrosion rate, whereas a value close to 0.5 indicates a high surface roughness due to a high metal dissolution and, thus, a high corrosion rate. Table 2 shows that both n_{ct} and n_f exhibit their highest values when 500 ppm of the inhibitor is added, whereas the lowest values are obtained at low and high inhibitor concentration.

The non-protective nature of the film formed on the steel immersed in the uninhibited 3.5 NaCl solution is evidenced in the micrograph shown in Figure 9, where a porous layer of corrosion products can be seen that consists mainly of the chemical elements present in the alloy such as Fe and C, along with oxygen. On the other hand, on steel corroded in the solution containing 500 ppm of the rare earths-based inhibitor, Figure 10, a much more compact film is observed although some parts of the uncovered steel can be seen, explaining why the inhibitor efficiency did not reach a value of 100%. Micro chemical analysis reveals the presence of F, O, Nd and Pr on the film formed on top of steel, indicating that the protective film contains oxides of iron and rare earths as reported in some other research papers [16–18]. For instance, Somers [16] evaluated La, Ce, Nd and Y 3-(4-methylbenzoyl)propionates (mbp) as corrosion inhibitors for mild steel in 0.01 M NaCl, finding that these compounds decreased the I_{corr} values by forming protective corrosion products and acted as predominantly anodic types of inhibitor. Peng [17] used La and Y 3-(4-methylbenzoyl)propionates for AS1020 mild steel in 0.01 M NaCl finding that the inhibition performance was due to the establishment of a protective film. Finally, Mohammedi [18] evaluated $Y(NO_3)_3 \cdot 6H_2O$ and $CeCl_3 \cdot 7H_2O$ in conjunction with metasilicates ($Na_2SiO_3 \cdot 5H_2O$) as corrosion inhibitors for carbon A37 steel in aerated 3% NaCl solution, finding that both anodic and cathodic reactions were inhibited leading to a decrease in the corrosion rate. Thus, the decrease in the I_{corr} values is due to the adsorption of rare earths containing inhibitor on the steel surface to form a protective film of corrosion products.

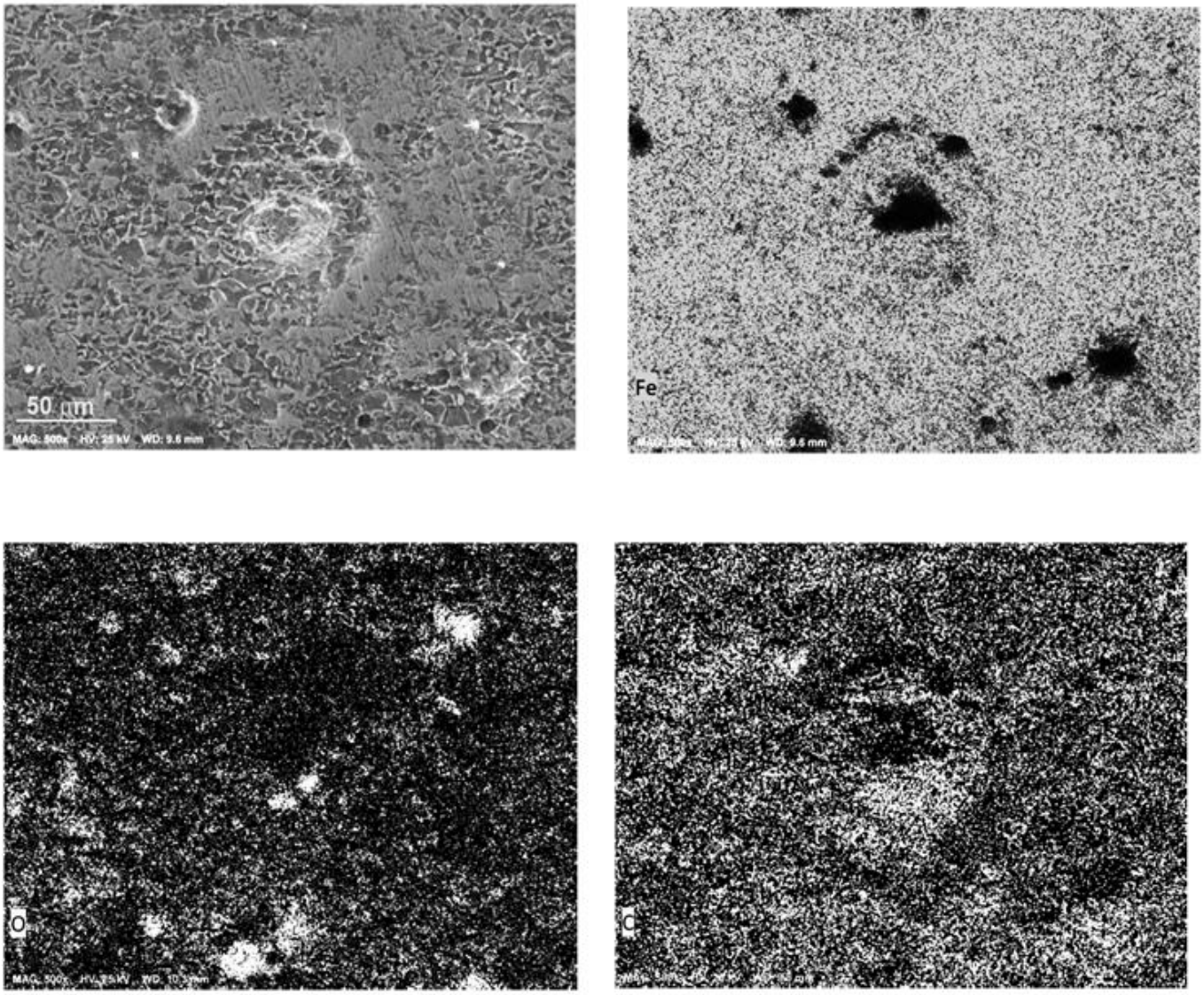

Figure 9. SEM micrographs of C-Mn steel corroded in 3.5% NaCl solution without the addition of the rare earth-based inhibitor together with EDS mappings of Fe, O and C.

Conclusions

- A compound containing neodymium and praseodymium sulphates, in a proportion of 65:35 approximately, has been synthetized from permanent magnets and used as a corrosion inhibitor for a C-Mn steel in 3.5% NaCl solution.
- This compound is a good corrosion inhibitor, with an efficiency that increases with time and with its concentration up to 500 ppm, but it decreases with a further increase in its concentration.
- Although this compound affects both anodic and cathodic electrochemical reactions, it has a stronger effect on the cathodic ones.

- This compound does not induce a passive layer, instead it forms a film of protective corrosion products by adsorbing chemically on the steel surface following a Langmuir adsorption isotherm.
- The corrosion process is charge transfer controlled and it is not altered by the inhibitor.

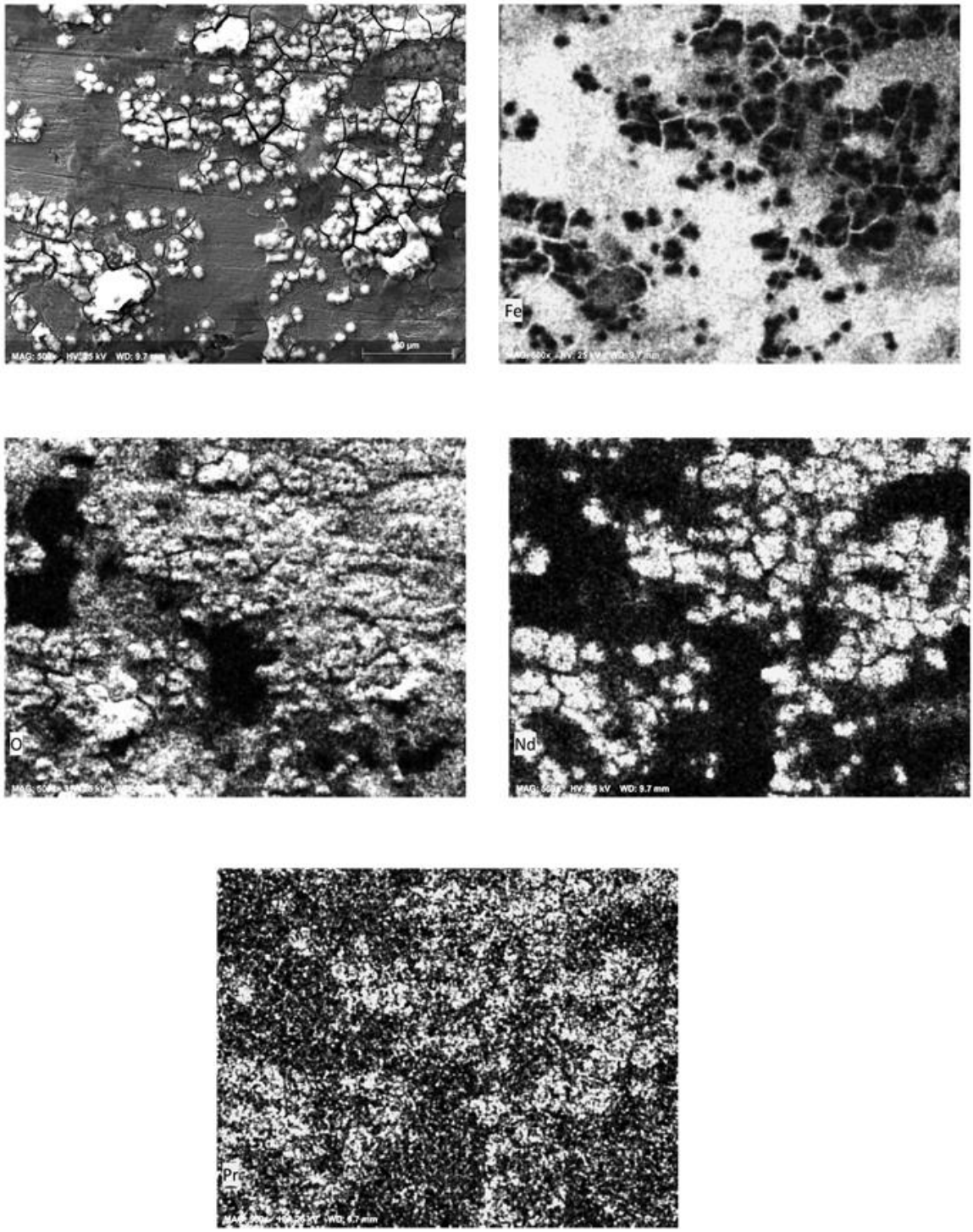

Figure 10. SEM micrographs of C-Mn steel corroded in 3.5% NaCl solution containing 500 ppm of the rare earth-based inhibitor together with EDS mappings of Fe, O, Nd and Pr.

References

1. S.D. Zhu, A.Q. Fu, J. Miao, Z.F. Yin, G.S. Zhou and J.F. Wei, Corrosion of N80 carbon steel in oil field formation water containing CO_2 in the absence and presence of acetic acid, *Corros. Sci*., 2011, **53**, no. 11, 3156–3165. doi: 10.1016/j.corsci.2011.05.059
2. M.K. Bagga, R. Gadi, O.S. Yadav, R. Kumar, R. Chopra and G. Singh, Investigation of phytochemical components and corrosion inhibition property of Ficus stem extract on mild steel in H_2SO_4 medium, *J. Environ. Chem. Eng*., 2016, **4**, no. 12, 4699–4707. doi: 10.1016/j.jece.2016.10.022
3. M.A. Al-Qudah, H.G. Al-Keifi, I.F. Al-Momani and S.T. Abu-Orabi, *Capparis Aegyptia* as a green inhibitor for aluminum corrosion in alkaline media, *Int. J. Corros. Scale Inhib*., 2020, **9**, no. 1, 201–218. doi: 10.17675/2305-6894-2020-9-1-12
4. H.I. Al-Itawi, G.M. Al-Mazaideh, A.E. Al-Rawajfeh, A.M. Al-Maabreh and A. Marashde, The effect of some green inhibitors on the corrosion rate of Cu, Fe and Al metals, *Int. J. Corros. Scale Inhib*., 2019, **8**, no. 2, 199–211. doi: 10.17675/2305-6894-2019-8-2-3
5. K.K. Anupama, K. Ramya, K.M. Shainy and A. Joseph, Adsorption and electrochemical studies of Pimenta dioica leaf extracts as corrosion inhibitor for mild steel in hydrochloric acid, *Mater. Chem. Phys*., 2015, **167**, 28–41. doi: 10.1016/j.matchemphys.2016.06.043
6. M.H. Hussin, A.A. Rahim, M.N.M. Ibrahim and N. Brosse, Improved corrosion inhibition of mild steel by chemically modified lignin polymers from *Elaeis guineensis* agricultural waste, *Mater. Chem. Phys*., 2015, **163**, 201–212. doi: 10.1016/j.matchemphys.2015.07.030
7. S. Bernal, F.J. Botana, J.J. Calvino, M. Marcos, J.A. Perez-Omil and H. Vidal, Lanthanide Salts as Alternative Corrosion Inhibitors, *J. Alloys Compd*., 1995, **225**, 638–641. doi: 10.1016/0925-8388(94) 07135-7
8. M. Bethancourt, F.J. Botan, M.A. Cauqui, M. Marcos, M.A. Rodríguez and J.M. Rodríguez-Izquierdo, Protection Against Corrosion in Marine Environments of AA5083 Al-Mg Alloy by Lanthanide Chlorides, *J. Alloys Compd*., 1997, **250**, 455–460. doi: 10.1016/S0925-8388(96)02826-5
9. M.A. Arenas, A. Conde and J.J. de Damborenea, Cerium: a suitable green corrosion inhibitor for tinplate, *Corros. Sci*., 2002, **44**, no. 3, 511–520. doi: 10.1016/S0010-938X(01)00053-1
10. A. Aballe, M. Bethencourt, F.J. Botana, M. Marcos, J. Perez and M.A. Rodríguez, Inhibidores de Escaso Impacto Medioambiental. Sistemas Basados en Tierras Raras, *Rev. Metal. (Madrid, Spain)*, 1997, **33**, no. 3, 363–369. doi: 10.3989/revmetalm.1997.v33.i6.770
11. A. Aballe, M. Bethencourt, F.J. Botana and M. Marcos, *$CeCl_3$ and $LaCl_3$* Binary Solutions as Environmental-Friendly Corrosion Inhibitors of AA5083 Al-Mg Alloy in NaCl Solutions, *J. Alloys Compd*., 2001, **323**, 855–858. doi: 10.1016/S0925-8388(01)01160-4

12. D. Ho, N. Brack, J. Scully, T. Markley, M. Forsyth and B. Hinton, Cerium Dibutylphosphate as a Corrosion Inhibitor for AA2024-T3 Aluminum Alloys, *J. Electrochem. Soc*., 2006, **153**, B392–B401. doi: 10.1149/1.2217260
13. K.F. Khaled, Electrochemical Evaluation of Environmentally Friendly Cerium Salt as Corrosion Inhibitor for Steel in 3.5% NaCl, *Int. J. Electrochem. Sci*., 2013, **8**, no. 9, 3974–3987.
14. D. Mohammedi, F. Ismail, R. Rehamnia, R. Bensalem and O. Savadogo, Corrosion Behaviour of Steel in the Presence of Rare Earth Salts: Synergistic Effect, *Corros. Eng., Sci. Technol*., 2015, **50**, no. 4, 633–638. doi: 10.1179/1743278215Y.0000000030
15. Y. Zhu, J. Zhuang, Y. Yu and X. Zeng, Research on Anti-Corrosion Property of Rare Earth Inhibitor for X70 Steel, *J. Rare Earths*, 2013, **31**, no. 6, 734–740. doi: 10.1016/S1002-0721(12)60350-0
16. B. Davó and J.J. de Damborenea, Use of rare earth salts as electrochemical corrosion inhibitors for an Al–Li–Cu (8090) alloy in 3.56% NaCl, *Electrochim. Acta*, 2004, **49**, no. 10, 4957–4965. doi: 10.1016/j.electacta.2004.06.008
17. A.E. Somers, B.R.W. Hinton, C. Bruin-Dickason, G.B. Deacon, P.C. Junk and M. Forsyth, New, environmentally friendly, rare earth carboxylate corrosion inhibitors for mild steel, *Corros. Sci*., 2018, **139**, 430–437. doi: 10.1016/j.corsci.2018.05.017
18. Y. Peng, A.E. Hughes, G.B. Deacon, P.C. Junk, B.R.W. Hinton, M. Forsyth and J.I. Mardel, A study of rare-earth 3-(4-methylbenzoyl)-propanoate compounds as corrosion inhibitors for AS1020 mild steel in NaCl solutions, *Corros. Sci*., 2018, **145**, 199–211. doi: 10.1016/j.corsci.2018.09.022
19. X.-B. Chen, T. Cain, J.R. Scully and N. Birbilis, Experimental Survey of Corrosion Potentials for Rare Earth Metals Ce, Er, Gd, La, and Nd as a Function of pH and Chloride Concentration, *Corrosion*, 2017, **70**, no. 3, 323–328. doi: 10.5006/1146
20. H. Allachi, F. Chaouket and K. Draoui, Protection against corrosion in marine environments of AA6060 aluminium alloy by cerium chlorides, *J. Alloys Compd*., 2010, **491**, 223–229. doi: 10.1016/j.jallcom.2009.11.042
21. F.O. Ogondo, I.D. Williams and T.J. Cherrett, How are WEEE doing? A Global Review of the Management of Electrical and Electronic Wastes, *Waste Manage*., 2011, **31**, no. 5, 714–730. doi: 10.1016/j.wasman.2010.10.023
22. K. Binnemans P.T. Jones, B. Blanpain, T. Van Gerven, Y. Yang, A. Walton and M. Buchert, Recycling of Rare Earths: A Critical Review, *J. Cleaner Prod*., 2013, **51**, no. 1, 1–22. doi: 10.1016/j.jclepro.2012.12.037
23. J. Porcayo-Calderon, J.J. Ramos-Hernandez, E. Porcayo-Palafox, L.M. Martınez de la Escalera, J. Canto, J.G. Gonzalez-Rodriguez and L. Martinez-Gomez, Sustainable Development of Corrosion Inhibitors from Electronic Scrap: Synthesis and Electrochemical Performance, *Adv. Mater. Sci. Eng*., 2019, 6753658. doi: 10.1155/2019/6753658
24. A. Olafsen and H. Fjellvag, Synthesis of rare earth oxide carbonates and thermal stability of $Nd_2O_2CO_3$ II, *J. Mater. Chem*., 1999, **9**, no. 11, 2697–2702. doi: 10.1039/A901988J

25. K. Rahmouni, M. Keddam, A. Srhiri and H. Takenouti, Corrosion of copper in 3% NaCl solution polluted by sulphide ions, *Corros. Sci*., 2005, **47**, no. 11, 3249–3266. doi: 10.1016/j.corsci.2005.06.017
26. P. Córdoba-Torres, T.J. Mesquita, O. Devos, B. Tribollet, V. Roche and R.P. Nogueira, On the intrinsic coupling between constant-phase element parameters α and Q in electrochemical impedance spectroscopy, *Electrochim. Acta*, 2012, **72**, 172–178. doi: 10.1016/j.electacta.2012.04.020

♦ ♦ ♦